Editors' Suggestion

Neutron-Resonance Transmission Analysis with a Compact Deuterium-Tritium Neutron Generator

Ethan A. Klein,[1] Farheen Naqvi,[1] Jacob E. Bickus,[1] Hin Y. Lee,[1] Areg Danagoulian,[1,*] and Robert J. Goldston[2]

[1] *Department of Nuclear Science and Engineering, MIT, Cambridge, Massachusetts 02139, USA*
[2] *Princeton Plasma Physics Laboratory, Princeton, New Jersey 08543, USA*

(Received 9 December 2020; revised 18 March 2021; accepted 16 April 2021; published 13 May 2021)

Neutron resonance transmission analysis (NRTA) is a spectroscopic technique that uses the resonant attenuation of epithermal neutrons to infer the isotopic composition of an object. NRTA is particularly well suited for applications requiring nondestructive analysis of objects containing mid- and high-Z elements. To date, NRTA has required large expensive accelerator facilities to achieve precise neutron beams and has not been suitable for on-site applications. In this study, we provide an experimental demonstration showing that NRTA can be performed using a compact low-cost deuterium-tritium (DT) neutron generator to analyze neutron resonances in the 1–50-eV range. The neutron transmission spectra for five single-element targets—silver, cadmium, tungsten, indium, and depleted uranium—each show uniquely identifiable resonant attenuation dips in measurement times on the order of tens of minutes. Closely spaced resonances of approximately 1-cm-thick multielement targets can be easily differentiated with 1-eV resolution up to neutron energies of 10 eV and 5-eV resolution up to neutron energies of 30 eV. These results demonstrate the viability of compact NRTA measurements for isotopic identification and have the potential to significantly broaden the applicability of the technique across materials science, engineering, and nuclear security.

DOI: 10.1103/PhysRevApplied.15.054026

I. INTRODUCTION

Most isotopes exhibit resonance behavior when interacting with neutrons. Some of the elements—many of them with mid-range and high atomic number Z—undergo resonance scattering, absorption, and fission in the epithermal regime of 1–100 eV. In this energy range, the resonances are sufficiently narrow and well separated that a given set of observed resonances constitutes a unique identifier of a particular isotope. Thus, spectroscopic measurement of neutron transmission and the resulting observation of attenuation dips in the transmitted spectrum can be used to infer the isotopic and elemental content of an unknown target. This is the basis of neutron resonance transmission analysis (NRTA).

In the past, NRTA has found applications in fields as broad as nuclear engineering, nuclear physics, and archaeology [1–11]. Furthermore, previous work in arms control has demonstrated the applicability of NRTA to problems of treaty verification [12,13]. Using pulsed neutron beams and time-of-flight (TOF) techniques, these applications have exploited the isotopic specificity of the NRTA signal. However, the high neutron fluxes and long beam lines necessary for sufficient spectral resolution have limited these applications to those that could be performed at facility-scale experimental setups. This circumstance has been a significant limitation to the broad applicability of an otherwise very powerful analytical technique. Recent work has sought to reduce the size of NRTA experimental setups by employing accelerator-based neutron sources; however, even these involve fairly large experimental facilities [14]. The prospect of using portable neutron generators and short beam lines has been raised [15] but no experimental results have yet been produced.

In this study, we provide an experimental demonstration showing that NRTA can be performed using relatively cheap, compact, and commercially available pulsed DT neutron generators, thereby expanding the potential applications of the technique. This effort requires a careful optimization of the moderator assembly and shielding to maximize the neutron output in the range of 1–100 eV and to reduce otherwise large neutron-scatter and neutron-capture backgrounds. Our past work via Monte Carlo (MC) simulations has indicated that such an approach is feasible [16]. NRTA applications using compact neutron sources can be further enhanced by applying the results from ongoing research into high-intensity pulsed DT and deuterium-deuterium (DD) neutron sources [17,18].

*aregjan@mit.edu

II. BACKGROUND

The NRTA technique involves analysis of the magnitude and energy of attenuation dips in neutron transmission spectra to reconstruct the isotopic composition of a target object. In combination with evaluated neutron cross-section data, the transmission spectrum can be used to estimate the linear density of the different isotopes present in the target object [8].

The total neutron cross section for a given material is a combination of both elastic potential scattering, which is nearly independent of energy, and resonant interactions, which are energy-dependent and specific to the isotopes present. At the resonance energies, the enhanced cross section of forming a compound nucleus in a particular excited state can be approximated by the single-level Breit-Wigner formalism [19]. According to this formalism, the cross section for compound nuclear formation by entrance channel α and subsequent reaction by exit channel β, $\sigma_{\alpha\beta}$, is given by

$$\sigma_{\alpha\beta}(E) = \frac{\pi}{k^2}\frac{\Gamma_\alpha\Gamma_\beta}{(E-E_{\rm res})^2+(\Gamma/2)^2}, \quad (1)$$

where Γ is the total decay width, Γ_α and Γ_β are the partial widths for the entrance channel α and exit channel β, respectively, k is the wave number, and $E_{\rm res}$ is the resonant energy [20]. At energies of 1–100 eV, the predominant resonant interaction is (n,γ), which results in absorption of the incoming neutron and observation of a dip in the neutron transmission spectrum.

Neutron transmission through a homogeneous target at a given incident energy, $T(E_n)$, will depend on the identities and areal densities of the isotopes present in the target and can be written as

$$T(E_n) = \frac{I(E_n)}{I_0(E_n)} = \exp\left(-\sum_i\sum_j n_i\sigma_{i,j}(E_n)\Delta x_i\right), \quad (2)$$

where $I(E_n)$ and $I_0(E_n)$ are the neutron fluxes measured at the detector for target-in and target-out setups, respectively, n_i is the atomic number density for isotope i, Δx_i is the target thickness for isotope i, and $\sigma_{i,j}(E_n)$ is the interaction cross section for isotope i and reaction j. This equation does not account for down-scattering and other secondary effects, which may become significant for thicker targets. In cases where these effects are significant, Monte Carlo N-particle (MCNP) simulations may provide a more accurate representation of neutron transmission for a given experimental setup.

Since the resonance energies and amplitudes are characteristic of the isotopes present in the target, the neutron transmission spectrum will be unique for a given target isotopic composition that includes isotopes with epithermal resonances, making it an isotopic geometric signature of a particular object, as described in Ref. [13]. Although some isotopes have individual resonances that are sufficiently close to those of another isotope such that the two cannot be distinguished, in most cases the combination of their multiple resonances can enable isotopic differentiation.

NRTA provides several benefits compared to gamma spectroscopy, including the ability to interrogate bulk high-Z material. NRTA can characterize any isotope that has sufficiently strong and well-resolved resonances in the neutron-energy region of interest and can also provide geometric information by using a position-sensitive detector [21–23]. This advantage is particularly important in arms-control applications [24] and is supported by the fact that many isotopes of interest to nuclear security (e.g., ^{235}U, ^{238}U, ^{239}Pu, and ^{240}Pu) exhibit (n,γ) and $(n,$fission) neutron resonances in the epithermal energy region (1–100 eV). The capability of NRTA to perform isotopic identification and quantification will be limited by the thickness of the target and the presence of any shielding.

III. EXPERIMENTAL TECHNIQUE

A. Experimental setup

The experiments are performed at the Vault Laboratory for Nuclear Science at MIT. A schematic diagram of the experimental setup is shown in Fig. 1. The neutron source is a portable A320 DT neutron generator, manufactured by Thermo Fisher Scientific Inc., that nominally generates 1×10^8 neutrons per second. The neutron generator is operated at a repetition rate of 5 kHz and a 5% nominal duty factor, with an acceleration voltage of 90 kV. Although the nominal pulse width is 10 μs, due to voltage rise times and plasma-formation time scales, the actual observed neutron pulse is only 3.3-μs wide following an initial 7-μs delay, as measured during experimental runs using the detector setup discussed in the next paragraph (see the inset of Fig. 2). These neutrons are produced nearly isotropically through the ^{3}H(^{2}H, n)^{4}He fusion reaction, with neutron energies of 14.1 MeV in the direction of the moderator. To moderate the emitted neutrons to the epithermal energy range, a 10.0-cm-thick high-density polyethylene (HDPE) hollow cylindrical moderator is placed radially around the DT tube. Surrounding the moderated source is 5%-borated polyethylene shielding, to reduce the neutron and gamma backgrounds.

All experiments discussed in this paper use a distance of 2.60 m from the tritium target in the DT tube to the front face of the detector. The front face of the moderator is located at an axial distance of 5.0 cm from the tritium disk, corresponding to a TOF distance of 2.55 m. MCNP simulations of the source-moderator assembly determine an effective moderation distance of 2.0 ± 0.1 cm, which, after adding to the true TOF distance, results in an effective TOF distance of 2.57 m.

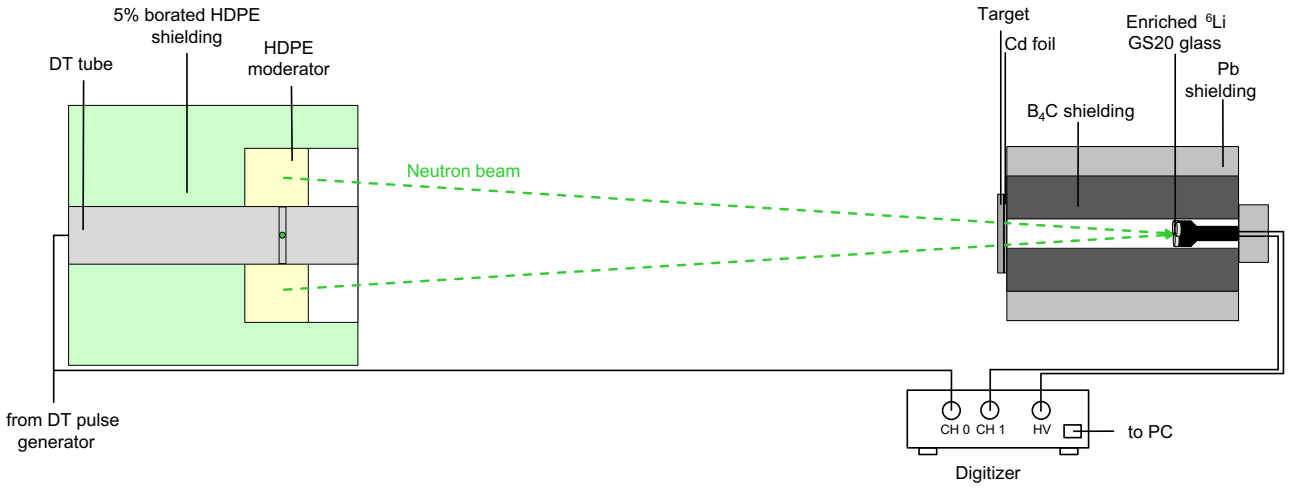

FIG. 1. A schematic of the experimental setup. The DT neutron generator is shielded by a box of borated plastic with a radial moderator composed of high-density polyethylene. The moderated neutron beam is incident on a target and detected in a 5-mm-thick ^{6}Li-enriched glass scintillator (GS20). Coupled to a photomultiplier tube. The neutron-generation signal and detector signal are both read out in a 14-bit 250-MS/s digitizer. The detector is shielded from neutrons by boron carbide and from photons by lead. Thermal wraparound neutrons are filtered by 3.0 mm of cadmium foil placed along the transmission axis.

The target objects are thin single-metal foils ranging from 0.0127 to 3.50 mm in thickness and of approximately 10 cm × 10 cm in area (see Table I). For targets containing W, Ag, and In, foils of 3.5-mm, 0.25-mm, and 0.0127-mm thickness are used, respectively. For depleted-uranium targets, individual 1.0-mm-thick foils are stacked to provide the desired target thickness. For targets containing multiple elements, the foils are stacked. The Cd foil is present for all sample runs (i.e., target-in) and for control runs with no target present (i.e., target-out) and is placed nearest to the detector (i.e., covering the collimator of the detector assembly).

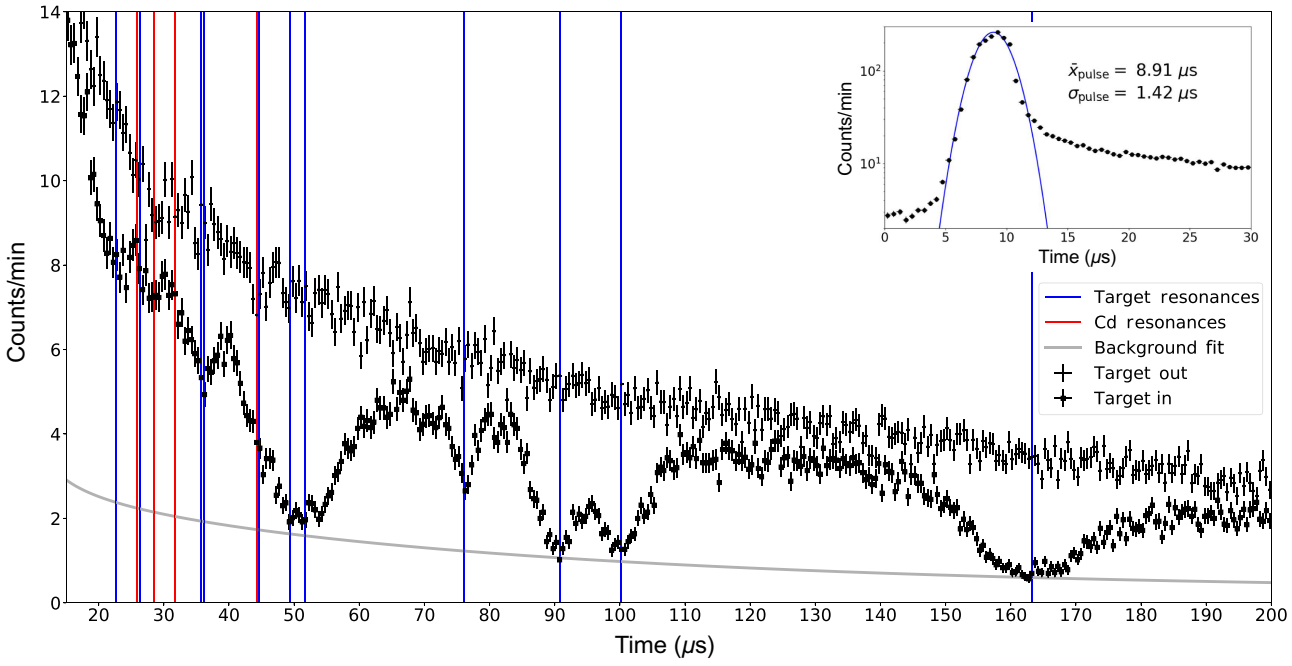

FIG. 2. The TOF distribution for a 2-h run with a 6.9-mm-thick composite target containing W, Ag, Cd, and In. The background fit, shown in gray, is performed according to the method discussed in Sec. IV A. The location of the expected resonance energies for target isotopes (blue lines) and the Cd foil (red lines) matches the location of the observed attenuation lines. The inset plots the total range of the neutron-generation pulse, showing the DT pulse at approximately 8.9 μs with a width of 1.4 μs.

TABLE I. The experimental targets.

Target[a]	Number of foils	Foil thickness (mm)
In, W, Ag	3	0.127, 3.5, 0.25
In	1	0.127
W	1	3.5
Ag	1	0.25
DU	5	1.0, 1.0, 1.0, 1.0, 1.0
W, Ag, DU, Pb	4	3.5, 0.25, 1.0, 1.1

[a]All target-in and target-out runs include the presence of a 3.0-mm Cd foil.

The detector setup consists of three circular 25.4 mm × 5 mm disks of ^{6}Li-enriched GS20 scintillator glass [25], placed horizontally adjacent to each other, optically mounted on a 76-mm-diameter Hamamatsu R1307-01 photomultiplier tube (PMT) with a Scionix VD 14–E1 base and operated at 1150 V. Neutrons are detected in the GS20 glass via the ^{6}Li$(n,^{3}\mathrm{H})^{4}$He reaction, depositing 4.78 MeV in the detector. This corresponds to a light output of approximately 1.6 MeV-electron-equivalent (MeVee) [26]. The GS20 glass does not contain any elements possessing epithermal neutron resonances in sufficient quantities to compete with the dominant neutron detection mechanism. The 5-mm thickness of the scintillator disks is chosen to maximize neutron detection efficiency, while reducing the probability of gamma interaction and maximizing light collection.

The detector and the PMT are placed within an aluminum box filled with boron carbide (B_4C) powder to shield thermal and epithermal neutrons, with a collimated opening in the front. The box is surrounded by 2-in-thick lead shielding to reduce the gamma background. The initiation signal of the DT pulse and the PMT signal are read into two channels of a 14-bit CAEN V1725 digitizer, which samples at the rate of 250 MS/s. Data acquisition is handled by the ADAQ toolkit [27] and the data are analyzed using both ROOT [28] and the SciPy [29] and ImagingReso [30] PYTHON libraries.

B. Background reduction

Accurate measurement of the neutron transmission requires reduction of the large backgrounds in the form of photons and unwanted neutron scattering within the detector assembly. The main source of gamma background is the $^{1}\mathrm{H}(n,\gamma)^{2}\mathrm{H}$ reaction in the moderator surrounding the DT source, producing 2.2-MeV photons that are detected on the time frame of neutron thermalization in the moderator (i.e., $\mathcal{O}$ (10 − 100 μs)). The digital signal analysis method of charge integration has been shown by others to improve neutron-gamma discrimination in the PMT response from GS20 scintillators by a factor of over 60 compared to pulse-height analysis [31] and so is chosen in this study to preferentially select neutron counts. As mentioned above, the thickness of the GS20 scintillator glass is chosen to be 5 mm to further reduce the photon contributions, while maintaining reasonable neutron detection efficiency (70% at 1 eV, 30% at 10 eV, and 10% at 100 eV). Another considerable background contribution to the detection of epithermal neutrons is that of the wraparound neutrons (i.e., slower neutrons incident on the detector during a subsequent pulse period). However, the detection of these neutrons can be significantly reduced by the use of a cadmium filter, as discussed later.

The surrounding of the detector with several centimeters of boron carbide powder reduces the thermal-neutron background by almost 99%. The impact of wraparound neutrons is minimized by a combination of a 200-μs pulse-repetition period and the placement of 3.0-mm cadmium foil on axis in front of the detector assembly. For the given pulse-repetition rate and a distance of 2.60 m between the moderator assembly and the detector, only neutrons with energies of approximately 0.75 eV and below could result in wraparound. The (n,γ) cross section of ^{113}Cd, a naturally occurring isotope, has a major broad resonance at 0.17 eV of 10 kb, which makes it an efficient material to absorb neutrons with energy below the approximately 0.75-eV wraparound cutoff. The utility of NRTA is not affected much by the presence of the cadmium foil, as very few isotopes have resonances below this cutoff (e.g., ^{151}Eu and ^{191}Ir). Furthermore, attenuation in the epithermal energy region due to 3.0-mm Cd is only approximately 6% and nearly independent of energy and since Cd has no resonances below 65 eV (aside from a weak resonance at 27.6 eV), measurement of neutron resonances in the target is not impeded.

C. TOF measurement

NRTA requires a means of measuring the neutron energy in order to reconstruct the neutron transmission as a function of the incident neutron energy. In these experiments, measurements of the neutron TOF are used to reconstruct the neutron energy. For a defined TOF path length, d_{TOF}, the following nonrelativistic kinematic relationship can be used to infer the neutron energy, E_n:

$$E_n = \frac{1}{2} m_n \left(\frac{d_{\mathrm{TOF}}}{t_{\mathrm{TOF}}}\right)^2, \tag{3}$$

where m_n is the neutron mass and $t_{\mathrm{TOF}} = t_{\mathrm{signal}} - t_{\mathrm{pulse}}$. Here, t_{signal} is the time of the detector trigger and t_{pulse} is the center time of the neutron-generation pulse. The resulting uncertainty in the neutron energy is given by

$$\frac{\Delta E_n}{E_n} = 2\sqrt{\left(\frac{\Delta t_{\mathrm{TOF}}}{t_{\mathrm{TOF}}}\right)^2 + \left(\frac{\Delta d_{\mathrm{TOF}}}{d_{\mathrm{TOF}}}\right)^2}, \tag{4}$$

where d_{TOF} is the TOF distance, Δd_{TOF} is the uncertainty in the TOF distance, and Δt_{TOF} is the uncertainty in the

TOF [32]. Given the $\mathcal{O}(\mu s)$ pulse width of the DT neutron generation and the chosen TOF distance, the energy uncertainty for this experimental setup is dominated by contributions from Δt_{TOF} across the entire 1–100-eV range. Thus, neutron sources with narrower pulses would be necessary in order to access absorption lines at energies much higher than 50 eV.

The uncertainty in the TOF, Δt_{TOF}, has contributions from the DT pulse width and the time resolution of the detector, which for a ^{6}Li glass scintillator is typically approximately 60 ns [31]. MCNP simulations show that the moderation time increases nonlinearly as a function of the final neutron energy, with a corresponding nonlinear uncertainty in moderation time. For this reason, the uncertainty in the moderation distribution is treated in terms of spatial uncertainty, rather than time uncertainty. The main source of the TOF uncertainty for this setup is thus due to the width of the DT pulse. For these experiments, the DT generator is set to produce a 10-μs pulse, the minimum pulse width possible for the A320 DT generator [33]. As discussed earlier, due to the plasma dynamics of neutron generation in the DT source, the actual width observed in neutron production is much shorter. The time distribution of the neutron generation is measured by observing the 0–20-μs region of each NRTA experimental run and fitting a Gaussian to the peak in detector signal and is found to be $\sigma = 1.41 \pm 0.06$ μs. Experiments using an EJ-309 liquid scintillator capable of pulse-shape discrimination confirm this peak to be a combination of neutron and gamma signals and validate the time profile of neutron generation as measured using the GS20 glass.

The uncertainty in the TOF distance is a result of the spatial spread of the neutrons following moderation from 14.1 MeV to epithermal energies. To minimize the impact of Δd_{TOF}, longer flight distances are preferred, but due to the reduction in neutron flux with distance, the need for reasonable measurement times sets a practical limit. A distance of 2.60 m, between the front face of the detector and the tritium disk within the DT tube, is thus chosen to support an acceptable TOF resolution while maintaining feasible measurement times. As mentioned above, for this experimental setup, this distance corresponds to an effective d_{TOF} of 2.57 m after accounting for neutron moderation. The TOF of approximately 1-eV neutrons is on the order of 185 μs for this distance, within the period of the DT neutron generator. Moderator studies using MCNP simulations have found the standard deviation in moderation distance to be 1.2 cm, leading to an overall uncertainty in the TOF distance of approximately 1.5 cm. Given the pulse width mentioned above, this contributes an uncertainty in the reconstructed neutron energy of < 0.1 eV in the epithermal range of interest and is not a limiting factor of the spectral resolution.

According to Eq. (4), the energy resolution for this experimental setup ($\Delta t_{\mathrm{TOF}} = 1.4$ μs and $\Delta d_{\mathrm{TOF}} = 1.5$ cm) is 0.02 eV at 1 eV, 5.3 eV at 50 eV, and 15 eV at 100 eV.

D. Data acquisition and processing

The data are acquired in a list mode, with one channel reading the signal pulses from the PMT coupled to the detector, while the other channel reads the initiation signal from the DT driving circuitry of the generator. In the postprocessing, each detector pulse is associated with a preceding TTL pulse and the TOF is calculated. As both channels use analog-to-digital converters driven by the same 250-MHz clock, this allows for determination of the signal time with an electronic precision of 4 ns. In addition to the TOF determination, it is necessary to further filter the data to reduce the gamma backgrounds that are present due to the photon sensitivity of the GS20 scintillator. By integrating the pulse area, a quantity proportional to the light output of the scintillator is computed. The distribution of signal-pulse areas is then analyzed to identify the main neutron peak due to the light output from alphas and tritons produced in the $^{6}\mathrm{Li}(n,\alpha)^{3}\mathrm{He}$ reaction in the scintillator. A Gaussian fit is performed and a $\pm 2\sigma$ cut is placed, thus significantly reducing the photon background. With the Cd filter in front and no target present, a data acquisition trigger rate of $<$200 Hz is observed in the ^{6}Li detector.

IV. RESULTS AND ANALYSIS

Experimental measurements ranging from 10-min to 2-h runs are performed for various target compositions of W, Ag, In, and depleted uranium (99.9% ^{238}U) ranging in thickness from 0.25 mm to 3.5 mm (see Table I). The raw counts within the neutron cut described in the previous section are normalized to counts per minute and binned with a 0.5-μs bin width. Figure 2 shows an example plot of a target consisting of In, W, and Ag in addition to the Cd-filter foil, along with the corresponding resonance energies from ENDF/B-VIII.0 libraries plotted as vertical lines [34]. Distinct absorption lines for indium, tungsten, and silver isotopes are clearly observable, as well as Cd lines in the target-out spectrum, allowing for subsequent element identification. As part of future work, the absolute concentrations of the isotopes can be extracted from this data—a goal that is particularly important for arms-control applications, where the enrichment of a fissile material is of importance.

A. Background correction

The background-reduction methods described in III B, in addition to the detector-pulse integral cut, eliminate most of the unwanted photon and scattered-neutron counts from the TOF spectrum. However, some residual background is present in the data, as observed at the bottoms

of attenuation dips, which should have zero counts due to the very high neutron cross sections. Therefore, an additional correction function is applied to the data to estimate and subtract the residual background.

The background is modeled using the "black-resonance" technique, where a strongly resonant target (e.g., tungsten, silver, or indium) is placed in the beam path and the background function is fitted to the bottom of the "saturated" attenuation dips. This technique is described in detail by Syme *et al.* [35]. A function of the following form is used following Fei *et al.* [10]:

$$B(t_m) = b_0 + b_1 e^{-t_m/\tau_1} + b_2 t_m^{-\tau_2}, \tag{5}$$

where t_m is the neutron detection time corrected for the median pulse time and b_0, b_1, b_2, τ_1, and τ_2 are fitting parameters. The first term in Eq. (5) accounts for constant background, the second accounts for the TOF distribution of 2.2-MeV γ from neutron capture on ^{1}H, and the third accounts for background due to neutrons that undergo elastic scattering within the detector assembly before detection.

This function is fitted to the resonance lines of a black-resonance target containing 0.127-mm In (1.46 eV), 3.5-mm W (4.15 eV, 18.84 eV), and 0.25-mm Ag (5.19 eV), measured during a dedicated 2-h run. To quantify the contributions of the 2.2-MeV photons, separate dedicated experiments are performed involving target-in and target-out runs using a $LaBr_3$ detector. A decay constant of $\tau_1 = 75 \pm 3$ μs is extracted using the $LaBr_3$ data and is used as a bound to the fit described by Eq. (5). With τ_1 thus determined, the neutron data are then fitted with Eq. (5) to determine the other parameters.

In applying the fit, attenuation of the background component from 2.2-MeV photons in the target must be taken into account. The photon attenuation in each target is calculated using the number densities and mass-attenuation coefficients [36] for each element present in the target and the ratio is taken to the attenuation in the "black-resonance" target used for the background fit. This correction is not applied to the neutron component of the target under the assumption that neutron scattering within the detector assembly would be independent of the target thickness, which is evidenced by statistical analysis of the best fit. Figure 2 shows the obtained fit function,

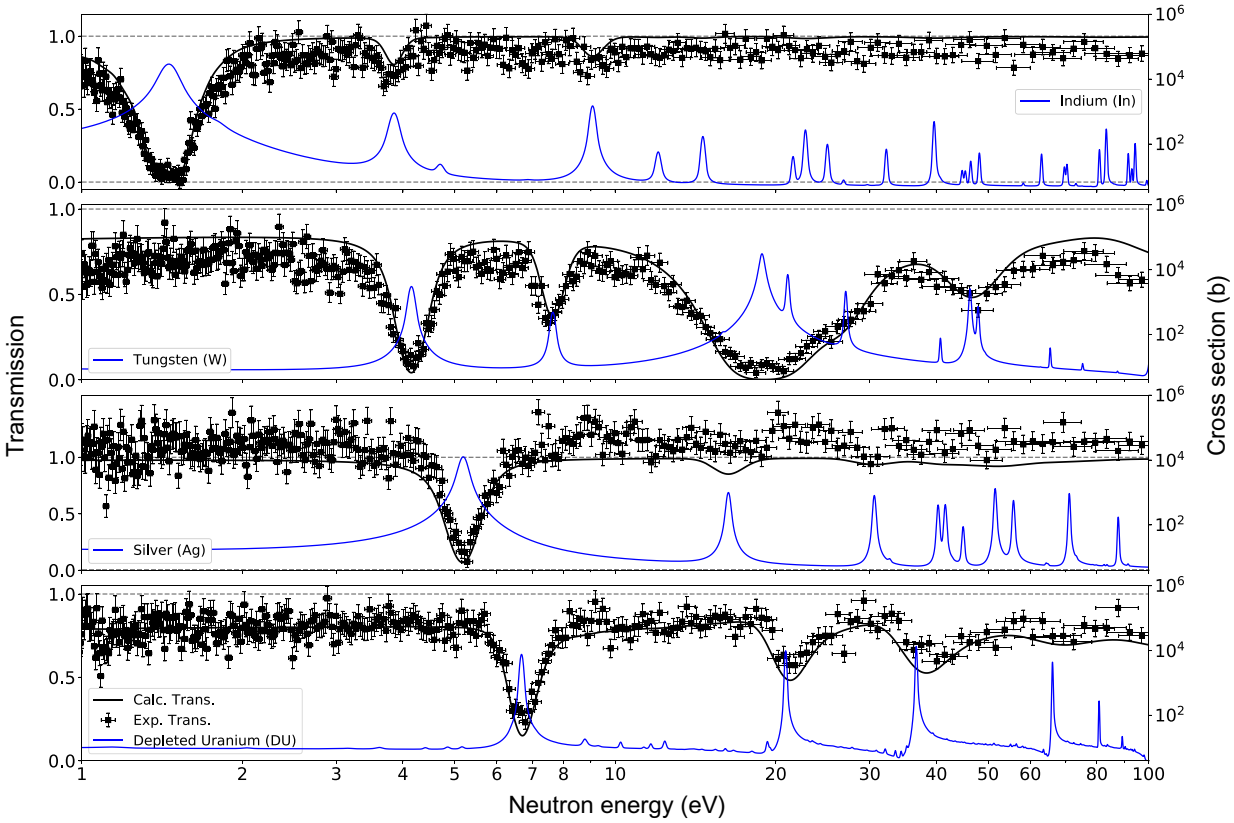

FIG. 3. The neutron cross-section and transmission data for single-element targets (from top to bottom, In, W, Ag, and depleted uranium). The measurement times are 2 h for all runs with the exception of Ag, which is a 1-h measurement. The experimental data are plotted along with the calculated transmission, which is a convolution of ENDF/B-VIII.0–evaluated neutron cross-section data with the pulse width of the DT neutron generation. The horizontal dotted lines demarcate zero transmission ($T = 0$) and full transmission ($T = 1$).

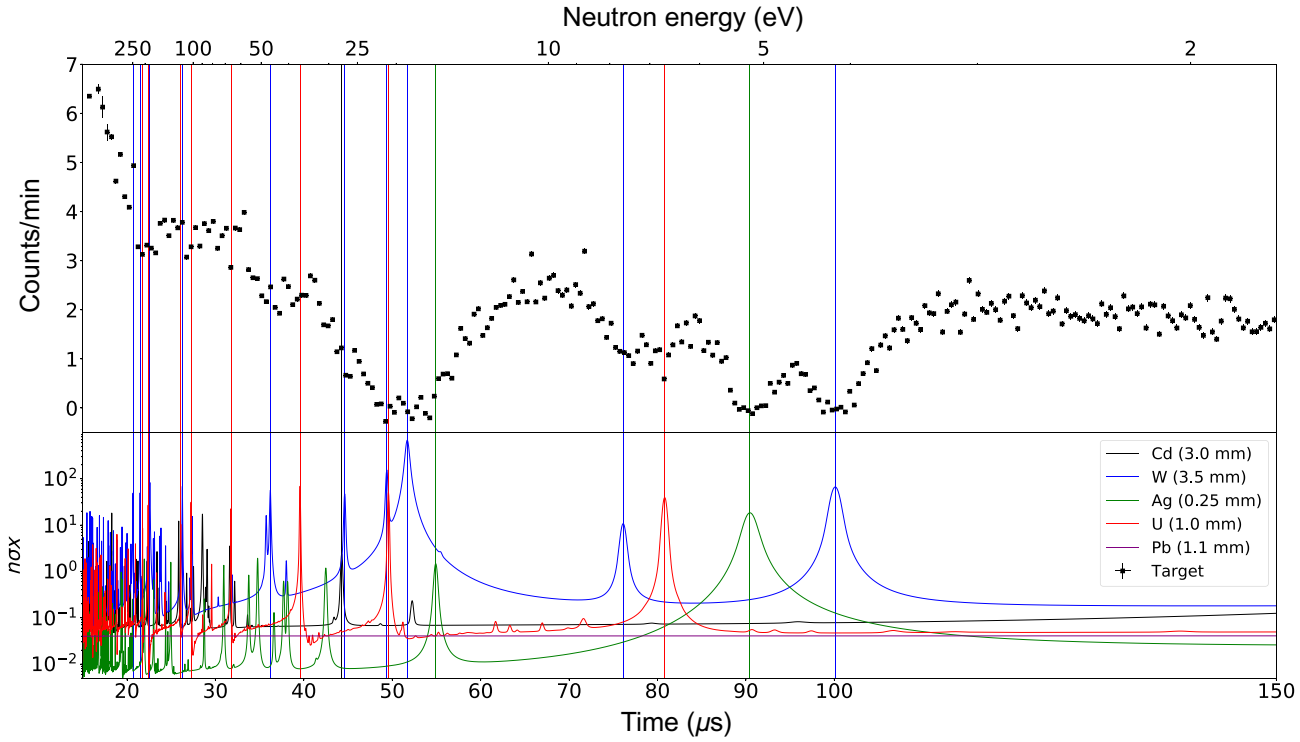

FIG. 4. The background-corrected transmitted neutron counts for a multielement target. The data are collected during a 2-h run with an 8.9-mm-thick target containing W, Ag, U, Pb, and Cd. The product of the total neutron cross section of each element with its number density and elemental thickness is plotted beneath. At low incident neutron energies (<10 eV), resonances within 1.0 eV are well resolved.

providing an estimate of the energy-dependent background counts that are then subtracted from the experimental data.

B. NRTA of single-element targets

Targets composed of a single mid- or high-Z element with strong neutron resonances are analyzed to measure the capability of the system to resolve resonances of varying widths across the epithermal energy range. The TOF histograms for target-in and target-out measurements are first background-corrected using the process described above and the target-out spectrum is filtered. Then, neutron transmission through the target is calculated by dividing the target-in histogram by the target-out histogram. Figure 3 shows the background-corrected neutron transmission for single-element targets and plots the elemental neutron cross section for comparison. The transmission is also computed by convolution of ENDF/B-VIII.0 cross-section data with the shape of the DT neutron pulse and is overlaid as the black line in the plot [34].

Neutron resonances of sufficient width can be identified up to 50 eV. Although this upper energy bound is much lower than that of fixed-facility NRTA setups, which can identify resonances up to the kiloelectronvolt range, the neutron transmission through each element presented here is clearly identifiable and matches the calculated transmission, demonstrating sufficiency for some isotopic identification applications. For nuclear-security and -safeguards applications, ^{238}U resonances at 6.7 eV, 20.9 eV, and 36.7 eV are well resolved and thus can be used to indicate the presence of ^{238}U in the target. Although the presence of ^{238}U can also be measured by gamma spectroscopy using the 1001-keV gamma emitted from ^{234m}Pa in the ^{238}U decay chain, determination of uranium enrichment can be challenging for thick or shielded objects. Gamma spectroscopy has been used for decades to accurately determine ^{235}U enrichment in samples [37] but the technique relies on measuring low-energy gammas (usually the 185.7 keV gamma from ^{235}U decay), which, due to their attenuation in high-Z materials, limits the interrogation to the surface of the target and not the bulk [38]. In contrast, neutrons interrogate the entire target and the resulting transmission spectrum is a product of interactions throughout the target, not just the surface.

The value of the reconstructed transmission is heavily dependent on the choice of the background-fit parameters and the target-out spectrum. While achieving good overall agreement, it can also be seen to diverge from the calculated transmission in nonresonant regions in some cases, by approximately 10%. This will not have an effect on elemental detection and attribution, as that goal primarily

depends on the observation of resonant dips. However, it could affect the quantification of the elemental concentration in the target, as it relies on the magnitude of the attenuation in the dip to that between the resonances to determine the isotopic number densities. Thus, future work should focus on better understanding and modeling of the backgrounds—e.g., via detailed Monte Carlo simulations—which would allow for a more precise determination of the transmission and more accurate estimations of the isotopic concentrations in the target.

C. NRTA of composite targets

Isotopic identification of multielement targets requires the ability to differentiate individual resonances. Figure 4 shows the background-subtracted transmission for a 2-h run with a composite target of W, Ag, Pb, and depleted-uranium foils (in addition to the fixed Cd foil). As can be seen from comparison to the elemental neutron cross sections, all resonances below 20 eV can be attributed to individual elements known to be present, whereas higher-energy resonances are observed but, due to their close spacing, are not always attributable to specific elements.

The spacing between the 20.9-eV resonance of ^{238}U and the 18.8-eV ^{186}W and 21.1-eV ^{182}W resonances is too close to resolve with the 3.3-μs-wide pulse of the DT generator. For that reason, nuclear-security applications requiring identification of ^{238}U in the presence of tungsten will have to rely on measuring the 6.7-eV ^{238}U resonance, unless narrower DT pulses are used (e.g., those achievable by a P235 DT portable neutron generator [39]) or a longer TOF distance is used with a corresponding increase in measurement time. If a longer TOF distance is chosen, it must be selected such that the TOF of the lowest-energy neutrons not attenuated by the Cd foil is smaller than the neutron-pulse period, in order to prevent wraparound neutrons. Similarly, given fixed constraints on duty cycles of portable neutron generators, a shorter neutron-generation pulse may correspond to a shorter pulse period, thus requiring a shorter TOF distance or a thicker Cd filter to prevent wraparound neutrons.

V. CONCLUSION

In this work, we demonstrate the feasibility of performing isotopic identification in under an hour with NRTA measurements using a compact DT generator and short TOF distances. The measurements show the resonant (n, n) elastic scattering and (n, γ) attenuation dips in the 1–50-eV range from medium- and high-Z elements. This compact and economic configuration can significantly increase the applicability of a powerful technique that, in the past, has been extremely limited due to the necessity of large accelerators and long neutron beam lines. This, in turn, would allow for practical applications in fields such as materials analysis, archaeology, and nuclear engineering. Verification of arms-control treaties in particular would benefit significantly from the use of such compact platforms in combination with already proven NRTA methods, as described in Refs. [12,13]. In addition, more intense neutron sources than the type used in this study may enable analysis of plutonium and fission products in spent nuclear fuel [1], another scenario where a compact NRTA setup for on-site analysis would be needed to limit the transport of special nuclear material.

In its current form, the technique does have a number of limitations and it would benefit from the following future improvements. The spectral resolution is limited by the 3.3-μs neutron-generation pulse, which reduces the ability to resolve absorption lines above 50 eV. The pulse can be shortened either by modifying the DT operation or by using more advanced faster-pulsed neutron sources such as those described in Refs. [18,39]. This is of particular importance when it comes to elements the powerful resonances of which below 50 eV result in the saturation of the absorption lines: to quantify the isotopic concentrations, one would need to observe and quantify the weaker higher-energy resonances. The technique is also limited by the presence of residual photon backgrounds from (n, γ) neutron capture inside the moderator. While energy-based filtering and background corrections are effective, the sensitivity could be further improved by using detectors with a higher ability to discriminate between neutron and photon counts. For example, Cs_2LiYCl_6 (CLYC) detectors appear promising in this regard [40,41]. Finally, these measurements would benefit from a more powerful pulsed neutron source, allowing for better statistics and shorter measurement times. Research is currently under way to develop such sources [17,42].

ACKNOWLEDGMENTS

This work was supported in part by U.S. Department of Energy Award No. DE-NA0003920, as part of the National Nuclear Security Administration (NNSA) Consortium of Monitoring, Technology, and Verification (MTV). E.A. Klein gratefully acknowledges NNSA support for this research, performed under appointment to the Nuclear Nonproliferation International Safeguards Fellowship Program sponsored by the Department of Energy, the National Nuclear Security Administration's Office of International Nuclear Safeguards (NA-241). We would like to thank our colleagues in the Consortium for MTV and in the MIT Department of Nuclear Science and Engineering for encouragement and advice.

[1] D. L. Chichester and J. W. Sterbentz, Assessing the feasibility of using neutron resonance transmission analysis (NRTA) for assaying plutonium in spent fuel assemblies, J. Nucl. Mater. Manage. (2012).

[2] M. A. Bourke, S. C. Vogel, S. L. Voit, K. J. Mcclellan, A. S. Losko, and A. Tremsin, *Non Destructive Examination of UN/U-*Si *Fuel Pellets Using Neutrons (Preliminary Assessment)*, Tech. Rep. (Los Alamos National Lab. (LANL), Los Alamos, NM (United States), 2016).

[3] P. Schillebeeckx, B. Becker, H. Harada, and S. Kopecky, in *Supplement to Volume I/24* (Joint Research Centre, European Commission, Luxembourg, 2015), p. 10.

[4] C. Andreani, G. Gorini, and T. Materna, in *Neutron Imaging and Applications*, edited by H. Bilheux, R. McGreevy, and I. Anderson (Springer, Boston, MA, 2009), p. 229.

[5] J. W. Sterbentz and D. L. Chichester, *Neutron Resonance Transmission Analysis (NRTA): A Nondestructive Assay Technique for the Next Generation Safeguards Initiative's Plutonium Assay Challenge*, Tech. Rep. (Idaho National Laboratory, 2010).

[6] A. Tremsin, S. Vogel, M. Mocko, M. Bourke, V. Yuan, R. Nelson, D. Brown, and W. Feller, Non-destructive studies of fuel pellets by neutron resonance absorption radiography and thermal neutron radiography, J. Nucl. Mater. **440**, 633 (2013).

[7] G. Festa, E. P. Cippo, D. Di Martino, R. Cattaneo, R. Senesi, C. Andreani, E. Schooneveld, W. Kockelmann, N. Rhodes, A. Scherillo, P. Kudejova, K. Biro, K. Duzs, Z. Hajnal, and G. Gorini, Neutron resonance transmission imaging for 3D elemental mapping at the ISIS spallation neutron source, J. Anal. At. Spectrom. **30**, 745 (2015).

[8] H. Hasemi, M. Harada, T. Kai, T. Shinohara, M. Ooi, H. Sato, K. Kino, M. Segawa, T. Kamiyama, and Y. Kiyanagi, Evaluation of nuclide density by neutron resonance transmission at the NOBORU instrument in J-PARC/MLF, Nucl. Instrum. Methods Phys. Res., Sect. A **773**, 137 (2015).

[9] C. Paradela, J. Heyse, S. Kopecky, P. Schillebeeckx, H. Harada, F. Kitatani, M. Koizumi, and H. Tsuchiya, in *EPJ Web of Conferences* (EDP Sciences, Bruges, Belgium, 2017), Vol. 146, p. 9002.

[10] F. Ma, S. Kopecky, G. Alaerts, H. Harada, J. Heyse, F. Kitatani, G. Noguere, C. Paradela, L. Šalamon, P. Schillebeeckx, H. Tsuchiya, and R. Wynants, Non-destructive analysis of samples with a complex geometry by NRTA, J. Anal. At. Spectrom. **35**, 478 (2020).

[11] G. Noguere, F. Cserpak, C. Ingelbrecht, A. Plompen, C. Quetel, and P. Schillebeeckx, Non-destructive analysis of materials by neutron resonance transmission, Nucl. Instrum. Methods Phys. Res., Sect. A **575**, 476 (2007).

[12] J. J. Hecla and A. Danagoulian, Nuclear disarmament verification via resonant phenomena, Nat. Commun. **9**, 1259 (2018).

[13] E. M. Engel and A. Danagoulian, A physically cryptographic warhead verification system using neutron induced nuclear resonances, Nat. Commun. **10**, 4433 (2019).

[14] Y. Kusumawati, I. Ozawa, Y. Mitsuya, T. Shiba, and M. Uesaka, X-band electron LINAC-based compact neutron source for nuclear debris on-site screening using short-distance neutron resonance transmission analysis, E-J. Adv. Maint. **11**, 46 (2019).

[15] H. Tsuchiya, F. Kitatani, M. Maeda, Y. Toh, and M. Kureta, Development of neutron resonance transmission analysis as a non-destructive assay technique for nuclear nonproliferation, Plasma Fusion Res. **13**, 2406004 (2018).

[16] E. M. Engel, E. A. Klein, and A. Danagoulian, Feasibility study of a compact neutron resonance transmission analysis instrument, AIP Adv. **10**, 015051 (2020).

[17] Starfire Industries, nGen™-400 PORTABLE NEUTRON INTERROGATION, http://www.starfireindustries.com/uploads/2/2/1/1/22111816/datasheet˙ngen-400˙rev01-19.pdf (2019), last accessed on 06.10.2019.

[18] Y. Podpaly, J. Hall, C. Goyon, P. Kerr, C. Chapman, C. Cooper, J. Mitrani, A. Povilus, B. Shaw, and A. Schmidt, *Environment Insensitive Detection of Fissionable Material with A Short Pulse Neutron Source*, Tech. Rep. (Lawrence Livermore National Lab. (LLNL), Livermore, CA (United States), 2018).

[19] J. Lynn, *The Theory of Neutron Resonance Reactions*, International Series of Monographs on Physics (Clarendon Press, 1968), https://books.google.com/books?id=-A95AAAAIAAJ.

[20] S. S. M. Wong, *Introductory Nuclear Physics* (Wiley Online Library, New York, 1990), Vol. 129.

[21] E. M. Schooneveld, M. Tardocchi, G. Gorini, W. Kockelmann, T. Nakamura, E. Perelli Cippo, H. Postma, N. Rhodes, and P. Schillebeeckx, A new position-sensitive transmission detector for epithermal neutron imaging, J. Phys. D: Appl. Phys. **42**, 1 (2009).

[22] A. S. Tremsin, W. B. Feller, and R. G. Downing, Efficiency optimization of microchannel plate (MCP) neutron imaging detectors. I. Square channels with ^{10}B doping, Nucl. Instrum. Methods Phys. Res., Sect. A **539**, 278 (2005).

[23] A. Tremsin, T. Shinohara, T. Kai, M. Ooi, T. Kamiyama, Y. Kiyanagi, Y. Shiota, J. McPhate, J. Vallerga, O. Siegmund, and W. Feller, Neutron resonance transmission spectroscopy with high spatial and energy resolution at the J-PARC pulsed neutron source, Nucl. Instrum. Methods Phys. Res., Sect. A **746**, 47 (2014).

[24] A. Losko, S. Vogel, M. Bourke, A. Tremsin, A. Favalli, S. Voit, and K. McClellan, in *Advances in Nuclear Nonproliferation Technology and Policy Conference* (American Nuclear Society, Santa Fe, NM, USA, 2016).

[25] Scintacor, the centre of scintillation, Cambridge CB4 0DL, United Kingdom, 6-lithium glass scintillators for neutron detection, https://scintacor.com/products/6-lithium-glass/.

[26] Y. Oshima, T. Yasumune, T. Masuda, K. Maehata, K. Ishibashi, and T. Umeno, Temperature dependence of Li-glass scintillator response to neutrons, Prog. Nucl. Sci. Technol. **1**, 296 (2011).

[27] Z. S. Hartwig, The ADAQ framework: An integrated toolkit for data acquisition and analysis with real and simulated radiation detectors, Nucl. Instrum. Methods Phys. Res., Sect. A **815**, 42 (2016).

[28] R. Brun and F. Rademakers, ROOT—an object oriented data analysis framework, Nucl. Instrum. Methods Phys. Res., Sect. A **389**, 81 (1997).

[29] P. Virtanen, *et al.*, SciPy 1.0: Fundamental algorithms for scientific computing in PYTHON, Nat. Methods **17**, 261 (2020).

[30] Y. Zhang and J.-C. Bilheux, ImagingReso: A tool for neutron resonance imaging, J. Open Source Softw. **407**, 1 (2017).

[31] C. A. Wang and R. A. Riedel, *Improved Neutron-Gamma Discrimination for a ^{6}Li-Glass Neutron Detector Using Digital Signal Analysis Methods*, Tech. Rep. (Instrument

and Source Division, Neutron Science Directorate, Oak Ridge National Laboratory, Oak Ridge, Tennessee 37831, USA).

[32] A. Brusegan, G. Noguere, and F. Gunsing, The resolution function in neutron time-of-flight experiments, J. Nucl. Sci. Technol. **39**, 685 (2002).

[33] Thermo Fisher Scientific Inc., MP 320 Neutron Generator, https://www.thermofisher.com/order/catalog/product/1517021A#/1517021A.

[34] D. Brown, M. Chadwick, R. Capote, A. Kahler, A. Trkov, M. Herman, A. Sonzogni, Y. Danon, A. Carlson, M. Dunn, D. Smith, and G. Hale, ENDF/B-VIII.0: The 8th major release of the nuclear reaction data library with CIELO-project cross sections, new standards and thermal scattering data, Nucl. Data Sheets **148**, 1 (2018), special Issue on Nuclear Reaction Data.

[35] D. B. Syme, The black and white filter method for background determination in neutron time-of-flight spectrometry, Nucl. Instrum. Methods Phys. Res. **198**, 357 (1982).

[36] J. Hubbell and S. Seltzer, Tables of x-ray mass attenuation coefficients and mass energy-absorption coefficients (version 1.4) (2010).

[37] R. Greenberg and B. Carpenter, High accuracy determination of ^{235}U in nondestructive assay standards by gamma spectrometry, J. Radioanal. Nucl. Chem. **111**, 177 (1987).

[38] D. Reilly, N. Ensslin, H. Smith, Jr., and S. Kreiner, *Passive Nondestructive Assay of Nuclear Materials*, Tech. Rep. (Nuclear Regulatory Commission, 1991).

[39] P325 Neutron Generator, a compact neutron generator for maximum versatility, http://www.thermo.com.cn/Resources/200802/productPDF˙24486.pdf (2019), last accessed on 02.12.2019.

[40] M. Bourne, C. Mussi, E. Miller, S. Clarke, S. Pozzi, and A. Gueorguiev, Characterization of the CLYC detector for neutron and photon detection, Nucl. Instrum. Methods Phys. Res., Sect. A **736**, 124 (2014).

[41] N. D'olympia, P. Chowdhury, C. Lister, J. Glodo, R. Hawrami, K. Shah, and U. Shirwadkar, Pulse-shape analysis of CLYC for thermal neutrons, fast neutrons, and gamma-rays, Nucl. Instrum. Methods Phys. Res., Sect. A **714**, 121 (2013).

[42] G. L. Kulcinski, R. F. Radel, and A. Davis, Near term, low cost, 14 MeV fusion neutron irradiation facility for testing the viability of fusion structural materials, Fusion Eng. Des. **109–111**, 1072 (2016), proceedings of the 12th International Symposium on Fusion Nuclear Technology-12 (ISFNT-12).